ACS OMEGA

http://pubs.acs.org/journal/acsodf

Article

The Development of New Catalytic Pigments Based on SiO_2 Amorphous Photonic Crystals via Adding of Dual-Functional Black TiO_{2-x} Nanoparticles

Li Feng, Hongjie Luo,* Fen Wang, Ting Zhao, Xiaohong Wei, Jianfeng Zhu, and Yi Qin*

Cite This: *ACS Omega* 2022, 7, 12089−12097

Read Online

ACCESS | Metrics & More | Article Recommendations

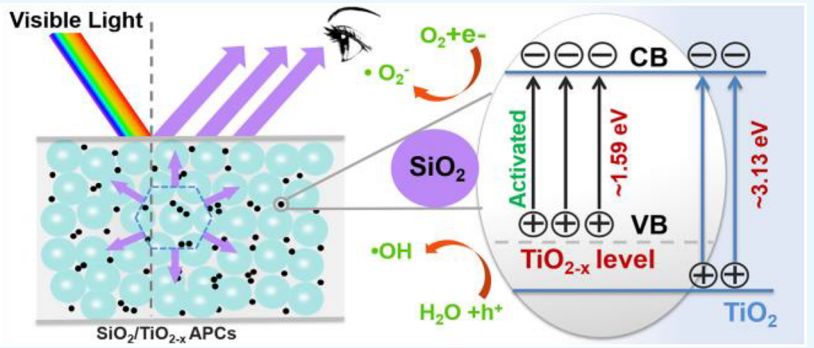

ABSTRACT: Biomimetic synthesis of amorphous photonic crystals (APCs) is an effective approach to obtaining non-iridescent structural colors. However, the structural colors of artificially prepared APCs are dim or even white due to the influence of incoherent scattering. In this paper, we present a novel method to combine APCs with black TiO_{2-x} to construct a noniridescent structural color pigments with high visibility and photocatalytic activity. Due to the absorption of incoherently scattered light by black TiO_{2-x}, the color saturation of structural colors has been significantly increased. In addition, the utilization rate of photogenic carriers was effectively enhanced by the slow light effect generated from the pseudoband gap of SiO_2 APCs with TiO_{2-x} absorbed full spectrum. The tone and color saturation of catalytic pigments is controlled by the diameter of SiO_2 nanospheres and the ratio of TiO_{2-x} nanoparticles, which provides a controllable application study in color-related fields as artwork, environmental coatings, and textiles.

1. INTRODUCTION

Color is an essential form of expression passed down through social civilization by integrating art and reality and expressing the complex emotions of human beings.[1,2] The human fascination with and pursuit of color never stop. From Dunhuang murals[3] to modern and fashionable decorative pigments,[4,5] humans continue to improve the color and visual effects of synthetic dyes. To find inspiration for synthetic pigments, people have paid attention to the brightly colored morpho butterfly,[6] peacock feathers,[7] and chameleons[8] that can switch colors instantly, which also inspired scientists to study the physics behind the appearance of colors. The sparkle of butterflies comes from the regular arrangement of scale cells. Bright color switching of the chameleon is caused by the combination of transparent guanine nanocrystals and melanosomes in the inner layer of the skin.[8−10] These submicron-scale materials are regularly arranged in a specific structure in space, and diffract, interfere, and scatter light at a particular wavelength, thus producing a structural color that will never fade.[10−13]

Structural color based on photonic crystals has bright color and an iridescent effect.[14,15] The angle-independent structural color prepared by the doping of melanin with amorphous photonic crystals (APCs) has been widely studied by scientists due to their soft colors and their ability to meet the visual needs of human beings.[16−18] The short-disordered APC structure produces incoherent scattering of light, which makes the color of the material white.[19] The current researchers introduced nanoscale carbon material (carbon, nanotube, acetylene black, and graphene) into the APC structure to absorb coherently scattered light or heat treatment in the presence of carbon in the reducing atmosphere to obtain

Received: January 18, 2022
Accepted: March 17, 2022
Published: April 1, 2022

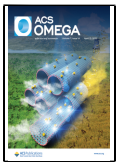

Scheme 1. Schematic Illustration of Preparation Strategy for SiO_2/TiO_{2-x} APCs Catalytic Pigments

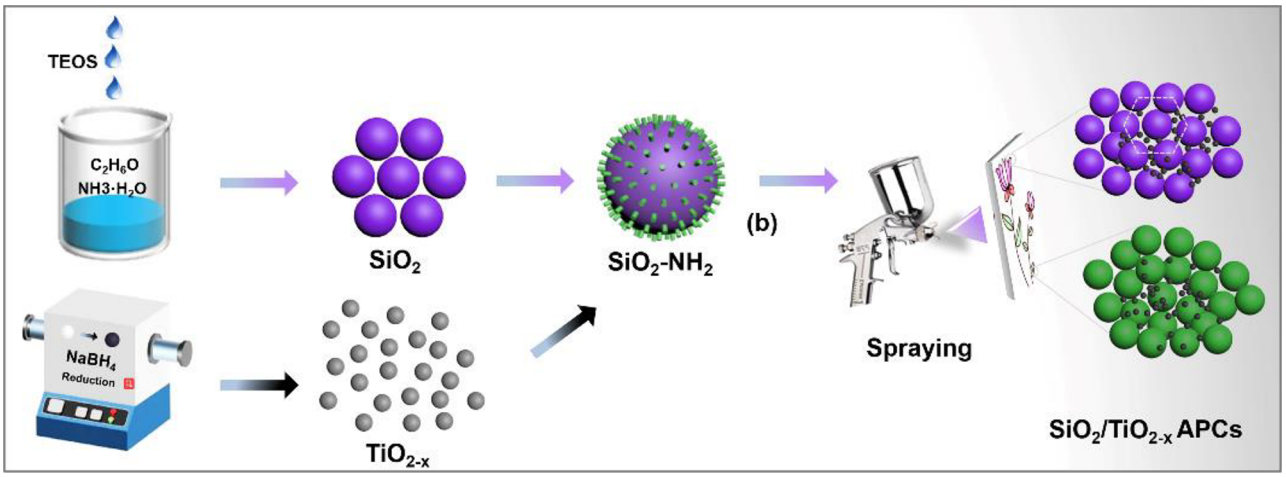

noniridescent structural color when synthesizing photonic crystal structure units.[20−23] Pastel colors and timeless noniridescent structural colors can replace traditional chemical colors in use. However, in the application process of home decoration coating, pigment, and other color decoration fields, it can still be used to reduce indoor environmental pollution.[24−28]

The well-known environmentally friendly material titanium dioxide (TiO_2) has excellent photocatalytic properties. Still, the white TiO_2 can only be excited to produce redox ability under ultraviolet light, which accounts for 5% of the light.[29−32] Therefore, the preparation of black TiO_{2-x} capable of full-spectrum absorption has become a research focus.[33,34] Hydrogen heat treatment of TiO_2, Al/Zn reduction of P25, hydrogen plasma reduction of TiO_2 nanotubes, and other preparation methods require high temperature and high pressure or are time-consuming, so the chemical reduction method is used to prepare TiO_{2-x}.[35−37] Black TiO_{2-x} particles effectively replace carbon black material and absorb coherently scattered light. Meanwhile, SiO_2 as a structural unit of APCs can effectively increase the specific surface area of TiO_2 to provide redox active sites. The black TiO_{2-x} has enhanced light absorption efficiency. The synergistic action of both can effectively promote the separation of electrons and holes and significantly enhance the photocatalytic effect on pollutants.[38−44]

Herein, black TiO_{2-x}, with excellent photocatalytic performance prepared after P25 was thermally reduced by $NaBH_4$, was used as a black additive to reduce incoherent scattering in APCs. A certain amount of TiO_{2-x} was added to the substrate by blending. In ethanol-activated SiO_2 nanospheres, TiO_{2-x} particles are distributed on the surface of the SiO_2 nanospheres after stirring for a certain period time at room temperature. After drying in a constant temperature drying oven at 50 °C, SiO_2/TiO_{2-x} APCs with photocatalytic properties and noniridescent structural color can be obtained. The preparation process is indicated in the schematic diagram (Scheme 1). Different colors can be adjusted by controlling the diameter of the SiO_2 nanospheres, and the color saturation can be governed by the amount of TiO_{2-x} added. The concentration of TiO_{2-x} is related to photocatalytic performance. Photocatalytic pigments have both decorative and environmental purification functions, which can effectively degrade the refractory toxic organic compounds produced in the color coatings decoration process. Therefore, the introduction of black TiO_{2-x} not only provides a direction for the functionalization of structural colors but also improves photocatalytic activity.

2. RESULTS AND DISCUSSION

2.1. Morphology and Structure of SiO_2/TiO_{2-x} APCs.

According to the Bragg diffraction law, the particle size of SiO_2 is related to the photonic bandgap of photonic crystals. Photonic bandgaps produced iridescent structural colors.[10,45] To obtain vivid color from the colloid assembly, it is essential to control the size of colloidal particles. First, SiO_2 nanospheres with different particle sizes were prepared using the improved Stöber method. The reaction mainly includes hydrolysis and polycondensation. The amount of TEOS (3 mL) and ammonia (4 mL) is fixed. The specific reagents used in the reaction are shown in Table 1. By controlling the concentration of ammonia and rate of TEOS hydrolysis, SiO_2 nanospheres with uniform size and different particle sizes were obtained.

Table 1. Size of SiO_2 Nanospheres

Sample	$NH_3·H_2O$	C_2H_5OH	TEOS	C_2H_5OH	Particle Size
1	4 mL	49 mL	3 mL	1 mL	221 nm
2	4 mL	45 mL	3 mL	5 mL	245 nm
3	4 mL	41 mL	3 mL	9 mL	287 nm

The SEM images of SiO_2 nanospheres with different particle sizes are shown in Figure 1a−c. The particle sizes of the obtained SiO_2 nanospheres are 221, 245, and 287 nm, respectively. SiO_2 distribution is uniform, and the particle surface is smooth and flat. The structural unit of APCs was prepared. When the amounts of TEOS and ammonia are unchanged, the particle size of SiO_2 depends on the ratio of ethanol. As the proportion of ethanol increases, the degree of alcoholysis for SiO_2 in ethanol increases, and SiO_2 crystal nuclei continue to grow, resulting in SiO_2 nanospheres with increased particle size. Short-range disordered SiO_2 APCs have a white appearance. They require black additives to absorb incoherently scattered light to eliminate the iridescent effect and achieve a single color used in pigments and inks.

As a new black additive, TiO_{2-x} is produced by the vacuum heat treatment of P25 (white TiO_2) and $NaBH_4$ in a tube

https://doi.org/10.1021/acsomega.2c00346
ACS Omega 2022, 7, 12089−12097

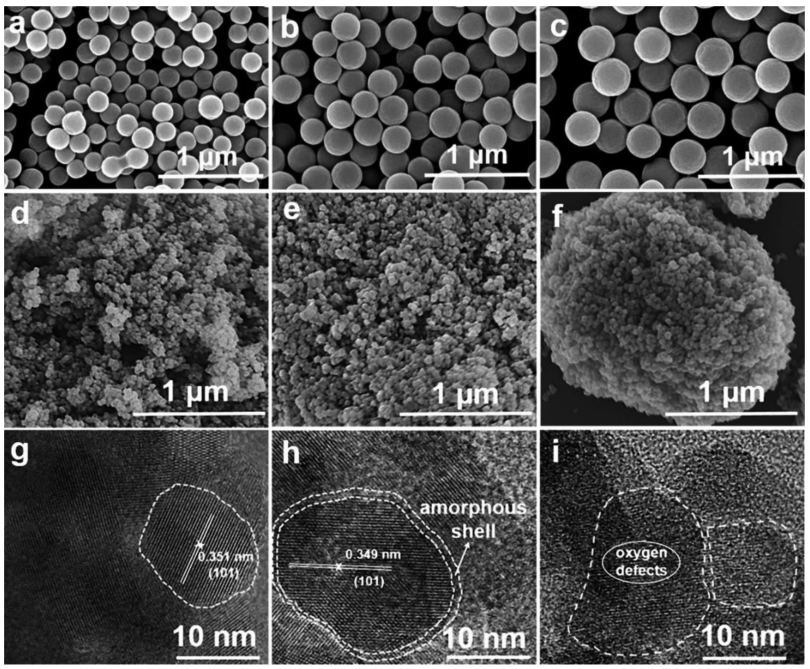

Figure 1. SEM images of SiO_2 nanospheres with different particle sizes (a–c). SEM (d–f) and TEM (g–i) images of TiO_{2-x} nanoparticles for different reductants (TiO_2:$NaBH_4$ = 4:0, 4:0.5, 4:0.75).

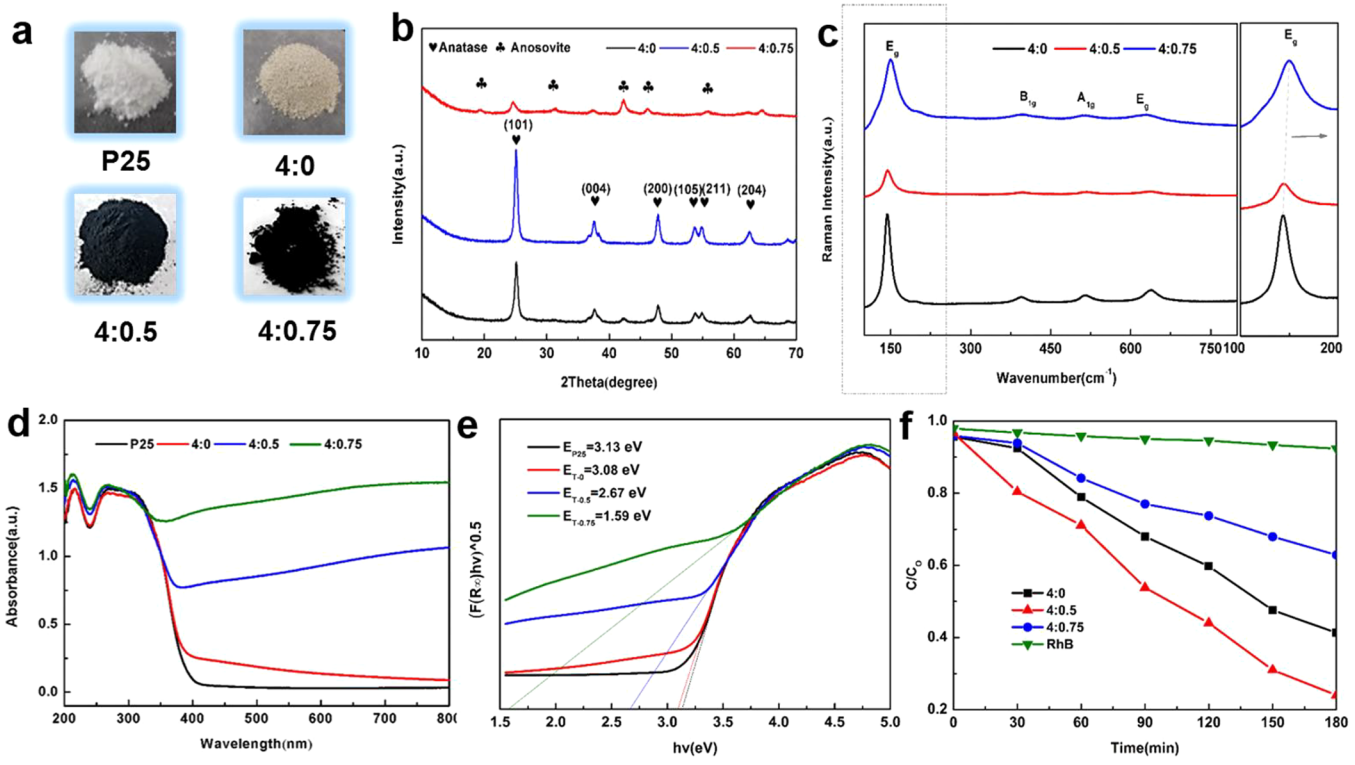

Figure 2. Macroscopic display of series samples (a). XRD patterns of TiO_{2-x} nanoparticles with different content of reductants (b). Raman diffraction spectrum of TiO_{2-x} (c). TiO_{2-x} samples and absorption spectra of reductants with different contents (d). Curve of $(Ahv)^{1/2}$–hv (e). Photocatalytic properties of TiO_{2-x} obtained with different reducing agents (f).

furnace to hypoxia. The morphology and structure of TiO_{2-x} were characterized by SEM, TEM, XRD, and Raman spectroscopy. The SEM and TEM of TiO_{2-x} obtained with different contents of reducing agent are shown in Figure 1d–i. The particle size of TiO_{2-x} without reducing agent is about 30 nm, and the dispersibility is better (Figure 1d–f). When 0.5 g of $NaBH_4$ was added for reduction, a portion of TiO_2 particles agglomerated, and the particle size increased. Some particles bonded together to form larger agglomerates. Figure 1g–i illustrates that before P25 is reduced, the TiO_2 nanocrystals exhibit a high degree of crystallinity and good lattice characteristics. Figure 1h testifies that the sample had a P25/

https://doi.org/10.1021/acsomega.2c00346
ACS Omega 2022, 7, 12089−12097

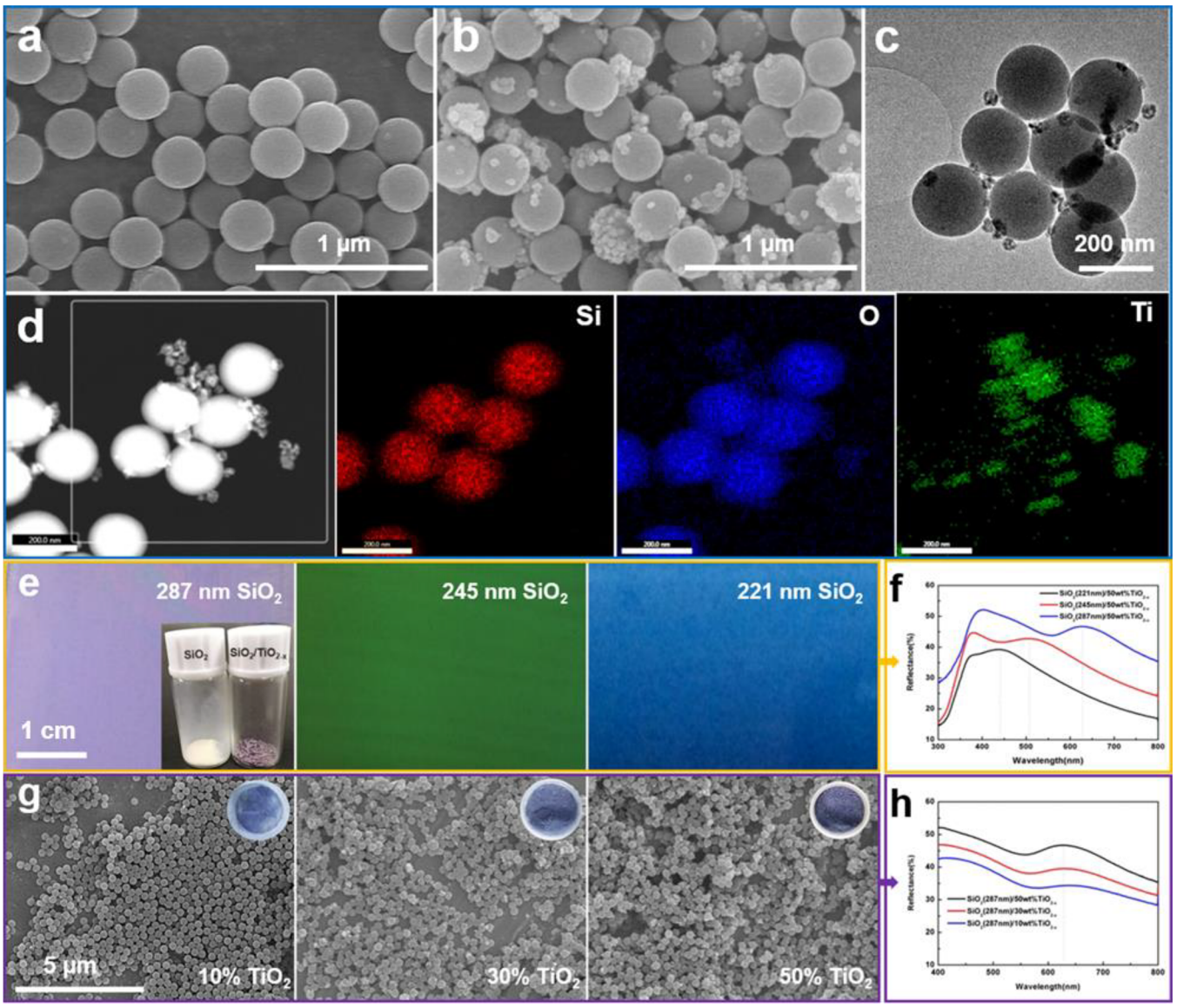

Figure 3. SEM of SiO_2 and SiO_2/TiO_{2-x} (a,b). TEM of SiO_2/TiO_{2-x} (c). EDS element analysis (d). Photos of SiO_2/TiO_{2-x} structural color with different particle sizes of SiO_2 (e), illustration of SiO_2 APCs and SiO_2/TiO_{2-x} APCs in (e). SEM of SiO_2/TiO_{2-x} (10%; (b): 30%; (c): 50%); the experimental sample is shown in the illustration (g). Reflection spectra of SiO_2/TiO_{2-x} APCs (f and h).

$NaBH_4$ mass ratio of 4:0.5 and reacted at 380 °C for 3 h. Samples showed a clear core−shell structure after $NaBH_4$ reduction; a highly crystalline inner core with an amorphous outer shell was observed. Figure 1i indicates that when the mass ratio was increased to 4:0.75, the proportion of amorphous shell in the sample in the entire crystal grain increased, and the thickness of shell also increased. As the degree of reduction increased, the inside of TiO_{2-x} lattice fringes became curved. With the thickening of the amorphous shell on the TiO_2 surface, the ordered lattice structure is almost invisible in the TEM image, and the lattice almost disappears.

The XRD and Raman spectra of crystal structure are shown in Figure 2. The XRD spectrum of TiO_{2-x} sintered at 380 °C at different ratios of P25 and $NaBH_4$ is illustrated in Figure 2b. At 380 °C, the diffraction peaks of two samples with a ratio of 4:0 and 4:0.5 appear at 2θ = 25.4°, 37.8°, 47.5°, 53.9°, 54.9°, and 62.4°, corresponding to anatase (101), (004), (200), (105), (211), and (204) crystal faces of mineral TiO_2 (JCPDS 21-1272), respectively. When the ratio of P25 to $NaBH_4$ is 4:0.75, the diffraction peak of the brookite phase appeared, indicating excess reducing agent at this time; TiO_2 was completely reduced to form Ti_2O_3 with a lower valence state. The Raman scattering spectrum characterization further illustrates the crystal structure of TiO_{2-x} series samples, as testified in Figure 2c. Four peaks appeared in the Raman diffraction pattern of colored TiO_2, 146, 394, 515, and 645 cm^{-1}, indicating that TiO_{2-x} and P25 have typical anatase phases. With the decrease in the molar ratio of P25 and $NaBH_4$, the degree of reduction of TiO_{2-x} increased. The concentration of oxygen vacancies gradually increased, and the thickness of amorphous shell increased. This is consistent with the phenomenon observed by TEM, indicating that with the increase in the degree of reaction, the concentration of oxygen vacancies and the thickness of amorphous shell increased.

This is consistent with the phenomenon observed by TEM, indicating that with the increase in the degree of reaction, the concentration of oxygen vacancies and the thickness of the

https://doi.org/10.1021/acsomega.2c00346
ACS Omega 2022, 7, 12089−12097

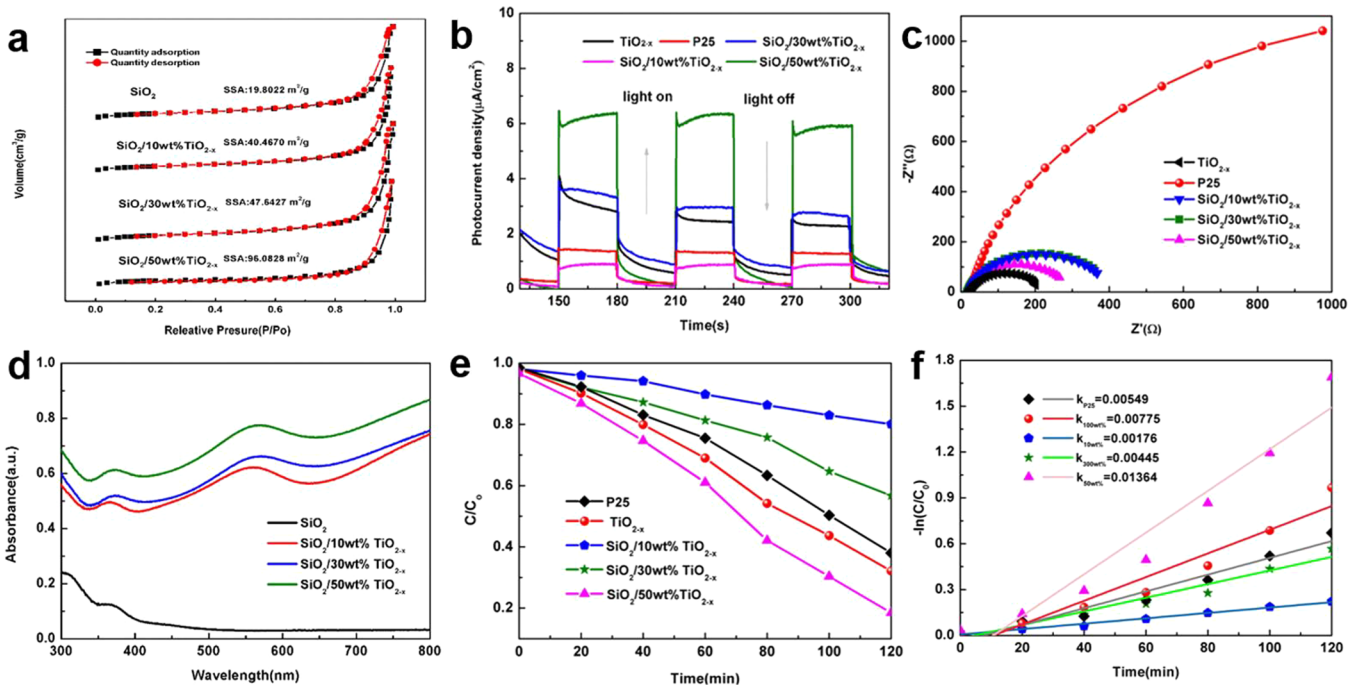

Figure 4. Nitrogen adsorption−desorption isotherm (a). Transient photocurrent responses (b). Nyquist plots of SiO_2/TiO_{2-x} sample (c). UV−vis absorption spectra (d). Photodegradation of SiO_2/TiO_{2-x} APCs (e,f).

amorphous shell increased. The peak corresponding to E_g shifted to the right and the phase changed, which shows that the molar mass ratio of TiO_2 to $NaBH_4$ is 4:0.5; the anatase phase and other phase samples exist. In a word, as the mass ratio decreases, the degree of TiO_2 reduction increases, the order of crystal lattice decreases, and the crystallinity decreases. Meanwhile, the thickness of the amorphous shell increases, and the color of TiO_2 deepens with the progress in reaction. Black TiO_{2-x} is more conducive to absorbing UV−vis light and acts as a black additive to absorb incoherent scattered light in APCs.

To rapidly and accurately analyze the light absorption mechanism of TiO_{2-x}, UV−vis diffuse reflectance analysis was performed for TiO_{2-x} samples prepared under different ratios. The results are demonstrated in Figure 2d. Untreated P25 showed strong absorption of UV light but weak absorption in the visible light range. TiO_{2-x} samples prepared by chemical reduction reaction not only showed strong absorption of UV light but also significantly increased the absorption of visible light, consistent with the results of other studies where it was found that an amorphous shell and Ti^{3+} enhance the absorbance through a synergistic effect. After improving the experimental method, the absorbance of TiO_{2-x} significantly changed. With the increase in $NaBH_4$, the appearance of TiO_{2-x} gradually darkened (yellow-black blue-black), and the performance shows that TiO_{2-x} powder not only gradually increased the absorption of visible light but also gradually increased the absorption of light in the near-infrared region. Especially, when the ratio of TiO_{2-x} and $NaBH_4$ was 4:0.5, the light absorption performance of TiO_{2-x} became significantly stronger in the full spectrum and showed the same absorption intensity for UV light, indicating that the reduction of TiO_2 substantially improved the material's absorption for different bands of light.

Calculation and analysis of bandgap showed that the reducing agent increased the reduction reaction of TiO_{2-x}, gradually darkening the appearance of catalyst. Meanwhile, the bandgap of catalysts decreased from 3.13 to 1.59 eV. The change in bandgap shown in Figure 2e indicates that the pigments have a corresponding response to the light of different bands. As the bandgap becomes smaller, the response of TiO_{2-x} to light gradually becomes stronger. It is imperative to acquire vividly visible structural colors.

In this experiment, by sequentially adjusting the ratio of P25 and $NaBH_4$ to 4:0, 4:0.5, and 4:0.75 and reducing in a vacuum tube furnace at 380 °C for 3 h, the colors of prepared TiO_{2-x} changed from white to black. This is because with the increase in the amount of $NaBH_4$, the concentration of reducing hydrogen increases by the thermal decomposition of $NaBH_4$, thereby increasing the concentration of intermediate (reducing hydrogen) required for the reduction reaction. When the concentration of intermediates increases, the reduction of iron dioxide intensifies simultaneously, and the reaction degree increases, increasing the oxygen vacancy of TiO_{2-x}. As a result, the oxygen vacancy of TiO_{2-x} increases. This is manifested in continuous color deepening (yellow−black−blue−black) on the macro level, and in turn the amorphous shell structure becomes thicker. Microscopically, more oxygen vacancies become available. However, an appropriate oxygen vacancy can promote the separation of electrons and holes, reduce the combination rate of electrons and holes, and improve the utilization rate of light.[46] The photocatalytic data are shown in Figure 2f. TiO_{2-x} shows a relatively strong degradation efficiency of RhB. Moderate reduction of $NaBH_4$ is beneficial to the improvement of photocatalytic efficiency.

2.2. Noniridescent Structural Color Analysis of SiO_2/TiO_{2-x} APCs. SiO_2/TiO_{2-x} APCs with photocatalytic activity and noniridescent structural colors were prepared from a mixture of TiO_{2-x} with excellent photocatalytic activity and activated 245 nm SiO_2 nanospheres. Their microscopic morphology was characterized by SEM, TEM, and EDS analyses, as shown in Figure 3a−d. TiO_{2-x} nanoparticles are

https://doi.org/10.1021/acsomega.2c00346
ACS Omega 2022, 7, 12089−12097

effectively loaded on the surface of SiO_2 and absorb the incoherent scattering in SiO_2 APCs, so that the non-iridescent structural colors generated by the pseudogaps of SiO_2/TiO_{2-x} APCs appear bright. Owing to the presence of incoherent scattering in APCs, the saturation of structural color is low. In this study, 10% TiO_{2-x} nanoparticles were added to SiO_2 colloidal particles and mixed with 10 mL ethanol to form a mixture, which was uniformly dispersed by ultrasonication and dried at 45 °C. Blue, green, and purple structural color materials were obtained, as shown in Figure 3e. The diameters of SiO_2 colloidal nanospheres are 221, 245, and 287 nm. The colors of SiO_2/TiO_{2-x} pigments prepared under different particle diameters of SiO_2 nanospheres are quite different, indicating that SiO_2 APCs have different colors. This is because the microstructure of APCs is long-range disordered and short-range ordered.

Nanospheres act as a structural unit, and the particle size affects the wavelength position of reflection peak, conforming to the Bragg−Snell law.[25] In addition, when the size of SiO_2 nanospheres gradually increases, the color of prepared structural color pigment starts to shift in the direction of long wavelength. Figure 3f shows that with the continuous increase in particle size, the position of reflection peak of powder moves to the long wavelength direction, and its reflection spectrum shows obvious characteristic peaks at 439, 512, and 635 nm. The total amount of reflection on both sides is low, consistent with the color observed with the naked eye. If the amount of TiO_{2-x} added is too low, the color of powder will be uneven and white. Therefore, the effect of 10%, 30%, and 50% TiO_{2-x} addition on the color was evaluated. With the increase in the amount of addition, the color gradually changed to dark green. By observing the morphology with SEM, it was found that with the increase in the amount of TiO_{2-x}, particle aggregation occurred at 50% (Figure 3g). However, as shown in Figure 3h, after SiO_2 with a particle size of 245 nm was introduced with different amounts of TiO_2, the position of the reflection peak did not move. Thirty nanometer TiO_{2-x} doping in the gap of 287 nm SiO_2 APCs does not affect the tone of the structure color, and it absorbs the incoherent scattering in APCs. 50% TiO_{2-x} doping level slightly reduces the reflectance of the structure color. Therefore, the addition amount of TiO_{2-x} can also be used to adjust the color saturation, increasing the application range of catalytic pigments.

2.3. Photocatalytic Activity and Enhanced Mechanism of SiO_2/TiO_{2-x} APCs. The active sites of photocatalytic materials are essential for the production of redox reactions. The large specific surface area increases the number of active sites. Figure 4a shows the N_2 adsorption−desorption isotherms of prepared TiO_{2-x} and SiO_2/TiO_{2-x}. According to the IUPAC classification, all the samples have similar type IV isotherms, and the relative pressure range is 0.7−0.95, producing a H3 hysteresis loop, a characteristic of mesoscopic materials.[26] In the range of (10, 30, and 50 wt %) TiO_{2-x}, the specific surface area increases with the increase in loading, significantly higher than TiO_{2-x}. SiO_2 provides dispersion sites for TiO_{2-x}, which can effectively increase the specific surface area of photocatalyst to increase the active site of photocatalytic reaction, and to facilitate the transmission of photogenerated carriers. The charge separation and transfer behavior of photocatalyst after light excitation can be analyzed by transient photocurrent and impedance measurements. Figure 4b shows the transient photocurrent response of the SiO_2/TiO_{2-x} sample. After 30 s of visible-light excitation, all the samples produced a constant current. The current of SiO_2/50 wt % TiO_{2-x} is 6.1 $\mu A/cm^2$, indicating that it has good charge separation efficiency and migration rate, which can be further explored. The semicircle in a high-frequency EIS diagram is a characteristic of the charge transfer process. The radius of the EIS semicircle is equal to the semiconductor charge transfer resistance. Figure 4c shows that the surface charge of TiO_{2-x} after chemical reduction is lower, almost five times smaller than that of P25. Meanwhile, with the increase in TiO_{2-x} content in SiO_2, the transfer resistance of SiO_2/TiO_{2-x} gradually decreased, indicating that SiO_2/TiO_{2-x} APCs can be used as photocatalysts. In summary, structural color and photocatalysis were achieved by integrating the functions of pigments. The UV−vis-NIR absorption spectrum is generally used to measure the light utilization rate of a substance. When the response to light is high, the utilization efficiency of the substance to light increases in the photocatalytic reaction. SiO_2 has almost no absorption of light, while after adding TiO_{2-x}, SiO_2/TiO_{2-x} has strong absorption characteristics in both UV and visible light (Figure 4d). With the increase of TiO_{2-x} addition, the absorption rate of SiO_2/TiO_{2-x} gradually increased. Because a pseudo band gap exists in the amorphous photonic crystal, its structural color is purple−red relative to 287 nm SiO_2/TiO_{2-x}, and double reflection peaks appear in the reflection spectrum. The corresponding reflection wavelengths are 406 and 635 nm. The absorption intensity decreased at 406 and 635 nm, but peaks appeared at 375 and 561 nm, caused by the edge effect of the photonic bandgap. Therefore, the introduction of TiO_{2-x} can enhance the light absorption. At the same time, the existence of pseudogaps of APCs produces a local optical effect and slow photon effect and synergistic enhancement of photon utilization ratio. Figure 4e illustrates the photocatalytic degradation curves of SiO_2/TiO_{2-x} prepared with 10%, 30%, and 50% introduction of RhB.

The introduction of black TiO_{2-x} into SiO_2 provided photocatalytic performance. SiO_2 APCs have no photocatalytic activity due to full transmittance to the light structure color. As the percentage of TiO_{2-x} increased, the rate of photodegradation of pollutants under simulated sunlight gradually increased. The photocatalytic degradation rate of SiO_2/50 wt % TiO_{2-x} is 0.03 min^{-1} (Figure 4f); compared with pure TiO_{2-x}, its photocatalytic degradation rate constant is 0.00775 min^{-1}, smaller than that for SiO_2/50 wt % TiO_{2-x}. As demonstrated in Scheme 2, the pseudogaps of APCs display the structural color, and the light localization effect and slow-light effect of pseudogaps promote photon absorption. Therefore, in this experiment, SiO_2/TiO_{2-x} APCs have a

Scheme 2. Schematic Diagram of the Enhancement Mechanism for Structural Color and Photocatalytic Performance of SiO_2/TiO_{2-x} APCs under Visible Light

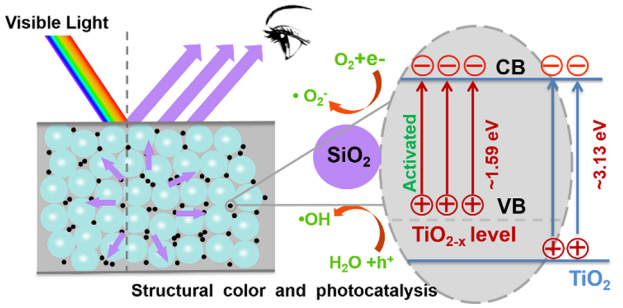

https://doi.org/10.1021/acsomega.2c00346
ACS Omega 2022, 7, 12089−12097

synergistic catalytic effect due to the optical localization effect and slow-light effect produced by the pseudogaps, and TiO_{2-x} with a large surface area, effectively enhancing the photocatalytic performance by improving the photon absorption.

3. CONCLUSION

By simulating the color rendering mechanism of the chameleon and promoting its functional application, we developed novel catalytic structural color pigments that not only provide vividly physical structural colors but also eliminate indoor pollutants. Black TiO_{2-x} with full-spectrum absorption prepared by reducing white TiO_2 with $NaBH_4$ was used as an additive to prepare noniridescent structural colors, achieving one-step synthesis of dual-functional SiO_2/TiO_{2-x} APCs. Compared with TiO_{2-x}, SiO_2/TiO_{2-x} APCs exhibited excellent photocatalytic activity. TEM characterization showed that SiO_2 nanospheres promoted the dispersion of TiO_{2-x} nanoparticles and provided active sites for catalytic reactions. DRS spectroscopy demonstrated that the slow-light effect produced by the pseudogaps of APCs promotes the photon utilization of catalytic pigment, improving the photoelectrochemical reaction and photocatalytic activity. Tone and color saturation of catalytic pigments can be controlled by adjusting the diameter of SiO_2 nanospheres and the ratio of TiO_{2-x}. This provides a basis for applying catalytic pigments in artwork, home decoration, and wall printing to decorate public places. Compared with traditional chemical pigments, these catalytic structural colors with decorative and photocatalytic functions can effectively satisfy the needs of mental and physical health.

4. EXPERIMENTAL METHODS

4.1. Fabrication of Dual-Functional SiO_2/TiO_{2-x} APCs. The detailed information on the reagents and characterization used in this study is listed as follows. Monodispersed SiO_2 was synthesized by the modified Stöber method.[47] Appropriate amounts of ethanol and tetraethoxysiliane (TEOS, 3 mL) were poured into the mixture of ethanol and ammonia (4 mL), and the solution was magnetically stirred at 40 °C to mix well. The homogeneous solution of ethanol and TEOS was added dropwise to the mixture of ethanol and ammonium hydroxide ($NH_3{\cdot}H_2O$, 4 mL), and the dropping rate was controlled at 0.2 mL/s. After the addition was completed, the system was continuously stirred at 40 °C and 500 rpm for 4 h to obtain white SiO_2 nanospheres. Second, the chemical reduction method was applied to prepare black TiO_{2-x}. P25 (4 g) and $NaBH_4$ were mixed for 30 min at room temperature. The mixture was placed into a combustion boat, the reduction reaction was carried out in a vacuum tube furnace, and the temperature was increased to 380 °C at a rate of 7 C/min for 2 h. A series of samples are obtained by controlling different molar ratios of P25 and $NaBH_4$ (4:0, 4:0.5, 4:0.75). The sample was washed with water to neutrality to remove unreacted $NaBH_4$, and then dried in an oven at 45 °C to obtain powdered black TiO_{2-x}. Finally, specific amounts of black TiO_{2-x} nanoparticles were added to the SiO_2 ethanol dispersion solution. A 50 mL dispersion was mixed by ultrasound for 4 h and stirred at room temperature for 7 h. Anhydrous ethanol and deionized water were centrifuged and dried in an oven at 50 °C to obtain SiO_2/TiO_{2-x} APCs with excellent photocatalytic activity and non-iridescent structural color.

4.2. Characterization and Photocatalytic Property Measurement of SiO_2/TiO_{2-x} APCs. The surface morphology of SiO_2/TiO_{2-x} APCs was observed by using field emission scanning electron microscopy (FESEM) (Hitachi FE-S4800). The reflection spectra and absorption spectra of SiO_2/TiO_{2-x} APCs pigments were measured by using a Cary 5000 UV−vis-NIR spectrometer (Agilen). The interplanar crystal spacing and crystalline structure of TiO_{2-x} nanoparticles were imaged by transmission electron microscopy (TEM, FEI Tecnai G2F20 S-TWIN) and X-ray diffraction (XRE; D/, ax-2200PC). The Raman scatting spectra of TiO_{2-x} were acquired with Renishaw-invia equipped with 532 nm red laser and CCD detector. The photocatalytic activity and photoelectrochemical analysis illustrate the ability to degrade pollutants. In the process of photocatalytic activity, 0.05 g SiO_2/TiO_{2-x} APCs catalytic pigments were added into 50 mL RhB solution (5×10^{-6} M) each time, which is probed by visible light irradiation from a BL-GHX-V photocatalytic reactor connected with a 500 W xenon lamp. Photoelectrochemical measurement was performed on an electrochemical workstation (CHI760E) using a normative three-electrode system, equipped with the Ag/AgCl electrode and platinum plate as the reference electrode and counter electrode, and the prepared photocatalysts as the working electrode. Two milligrams of photocatalyst was added to the mixture of 0.5 mL dimethylformamide and 1 mL ethanol to acquire the emulsion, which was coated in 1.0 cm^3 FTO glass as the working electrode. Electrolyte is 0.5 M $NaSO_4$ aqueous solution. The photocurrent curve was remarked by amperage under intermittent irradiation. Electrochemical impedance spectroscopy (EIS) was obtained in the frequency range of 0.01−100,000 Hz.

AUTHOR INFORMATION

Corresponding Authors

Hongjie Luo − *Shaanxi Key Laboratory of Green Preparation and Functionalization for Inorganic Materials, School of Materials Science and Engineering, Shaanxi University of Science and Technology, Xian, Shaanxi 710021, China; School of Materials Science and Engineering, Shanghai University, Shanghai 200444, China*; Email: hongjieluo@shu.edu.cn

Yi Qin − *Shaanxi Key Laboratory of Green Preparation and Functionalization for Inorganic Materials, School of Materials Science and Engineering, Shaanxi University of Science and Technology, Xian, Shaanxi 710021, China*; orcid.org/0000-0001-8245-8207; Email: qinyi@sust.edu.cn

Authors

Li Feng − *Shaanxi Key Laboratory of Green Preparation and Functionalization for Inorganic Materials, School of Materials Science and Engineering, Shaanxi University of Science and Technology, Xian, Shaanxi 710021, China*

Fen Wang − *Shaanxi Key Laboratory of Green Preparation and Functionalization for Inorganic Materials, School of Materials Science and Engineering, Shaanxi University of Science and Technology, Xian, Shaanxi 710021, China*; orcid.org/0000-0003-1035-2205

Ting Zhao − *Shaanxi Key Laboratory of Green Preparation and Functionalization for Inorganic Materials, School of Materials Science and Engineering, Shaanxi University of Science and Technology, Xian, Shaanxi 710021, China*

https://doi.org/10.1021/acsomega.2c00346
ACS Omega 2022, 7, 12089−12097

Xiaohong Wei − *Shaanxi Key Laboratory of Green Preparation and Functionalization for Inorganic Materials, School of Materials Science and Engineering, Shaanxi University of Science and Technology, Xian, Shaanxi 710021, China*

Jianfeng Zhu − *Shaanxi Key Laboratory of Green Preparation and Functionalization for Inorganic Materials, School of Materials Science and Engineering, Shaanxi University of Science and Technology, Xian, Shaanxi 710021, China*

Complete contact information is available at: https://pubs.acs.org/10.1021/acsomega.2c00346

Author Contributions

L. Feng performed the ab initio experimental design and data compilation. L. Hong and Y. Qin conceived and designed the experiments. All authors were involved in the discussion and writing of the manuscript.

Notes

The authors declare no competing financial interest.

Data Availability: All data required for the conclusions in the paper are presented in the paper and in the Supporting Information. Additional data relevant to this thesis may be obtained from the corresponding authors upon reasonable request.

■ ACKNOWLEDGMENTS

All authors have given approval to the final version of the manuscript. This work was supported by the National Key R&D Program of China (2019YFC1520202) and the National Natural Science Foundation of China (No. 51702193, 51502165, 51972201).

■ REFERENCES

(1) Morales-Oyervides, L.; Oliveira, J.; Sousa-Gallagher, M.; Méndez-Zavala, A.; Cesar Montañez, J. Assessment of the dyeing properties of the pigments produced by talaromyces spp. *J. Fungi (Basel)* **2017**, *3*, 38.

(2) Wang, L.; Li, Q. Photochromism into nanosystems: towards lighting up the future nanoworld. *Chem. Soc. Rev.* **2018**, *47*, 1044−1097.

(3) Liang, J.; Wan, X. Prototype of a pigments color chart for the digital conservation of ancient murals. *J. Electron. Imaging* **2017**, *26*, 023013.

(4) Mishra, M. K.; Schöttle, C.; Van, D. A.; Beshah, K.; Bohling, J.; Roper, J.; Radke, C.; Katz, A. Wettability reversal of hydrophobic pigment particles comprising nanoscale organosilane shells: Concentrated aqueous dispersions and corrosion-resistant waterborne coatings. *ACS Appl. Mater. Interfaces* **2019**, *11*, 44851−44864.

(5) Ravi, S. K.; Udayagiri, V. S.; Suresh, L. Emerging role of the band-Structure approach in biohybrid photovoltaics: A path beyond bioelectrochemistry. *Adv. Funct. Mater.* **2018**, *28*, 1705305.

(6) Yoshioka, Y.; Shimizu, S.; Kinoshita, S.; Matsuhana, B. Structural color of a lycaenid butterfly: analysis of an aperiodic multilayer structure. *Bioinspir. Biomin.* **2013**, *8*, 045001.

(7) Freyer, P.; Wilts, B. D.; Stavenga, D. G. Reflections on iridescent neck and breast feathers of the peacock Pavo cristatus. *Interfaces Focus* **2019**, *9*, 20180043.

(8) Teyssier, J.; Saenko, S. V.; Dirk, V. D. M.; Milinkovitch, M. C. Photonic crystals cause active colour change in chameleons. *Nat. Commun.* **2015**, *6*, 6368.

(9) Wang, Y.; Cui, H.; Zhao, Q.; Xuemin, D. Chameleon-inspired structural-color actuators. *Matter* **2019**, *1*, 626−638.

(10) Wu, P.; Wang, J.; Jiang, L. Bio-inspired photonic crystal patterns. *Mater. Horiz.* **2020**, *7*, 338−365.

(11) Kinoshita, S.; Yoshioka, S.; Miyazaki, J. Physics of structural colors. *Rep. Prog. Phys.* **2008**, *77*, 076401.

(12) Hu, Y.; Zhang, Y.; Yang, D.; Ma, D.; Huang, S. Self-assembly of colloidal particles into amorphous photonic crystals. *Mater. Adv.* **2021**, *2*, 6499−6518.

(13) Seago, A.; E Seago, E. A.; Oberprieler, R.; Saranathan, V. K. Evolution of insect iridescence: origins of three-dimensional photonic crystals in weevils (Coleoptera: Curculionoidea). *Integr. Comp. Biol.* **2019**, *59*, 1664−1672.

(14) Mika, F.; Matějková-Plšková, J.; Jiwajinda, S. Photonic crystal structure and coloration of wing scales of butterflies exhibiting selective wavelength iridescence. *Materials (Basel)* **2012**, *5*, 754−771.

(15) Aguirre, C. I.; Reguera, E.; Stein, A. Colloidal photonic crystal pigments with low angle dependence. *ACS Appl. Mater. Interfaces* **2010**, *2*, 3257−3262.

(16) Meng, M.; Umair, M.; Iqbal, K.; Xin, J.; Zhang, S.; Tang, B. Rapid fabrication of noniridescent structural color coatings with high color visibility, good structural stability, and self-healing properties. *ACS Appl. Mater. Interfaces* **2019**, *11*, 13022−13028.

(17) Liu, P.; Chen, J.; Zhang, Z.; Xie, Z.; Du, X.; Gu, Z. Bio-inspired robust non-iridescent structural color with self-adhesive amorphous colloidal particle arrays. *Nanoscale* **2018**, *10*, 3673−3679.

(18) Zhao, Y.; Xie, Z.; Gu, H. Bio-inspired variable structural color materials. *Chem. Soc. Rev.* **2012**, *41*, 3297−3317.

(19) Shi, L.; Zhang, Y.; Dong, B.; Zhan, T.; Liu, X.; Zi, J. Amorphous photonic crystals with only short-range order. *Adv. Mater.* **2013**, *25*, 5314−5320.

(20) Kim, H.; Kang, B.; Cui, X.; Lee, S. K.; Lee, W.; Cho, D.; Woonbong, H.; Tim, B. F.; Woodfield, K. S. L.; Jang, J. Light-activated decellularized extracellular matrix-based bioinks for volumetric tissue analogs at the centimeter scale. *Adv. Funct. Mater.* **2021**, *31*, 2104991.

(21) Wang, F.; Zhang, X.; Lin, Y.; Wang, L.; Zhu, J. Structural coloration pigments based on carbon modified ZnS@SiO_2 nanospheres with low-angle dependence, high color saturation, and enhanced stability. *ACS Appl. Mater. Interfaces* **2016**, *8*, 5009−5016.

(22) Liu, Y.; Wang, Y.; Wang, Y.; Shu, Y.; Tan, H.; Zhao, Y. Bioinspired structural color particles with multi-layer graphene oxide encapsulated nanoparticle components,. *Bioact. Mater.* **2020**, *5*, 917−923.

(23) Li, F.; Tang, B.; Xiu, J.; Zhang, S. Hydrophilic modification of multi-walled carbon nanotube for building photonic crystals with enhanced color visibility and mechanical strength. *Molecules* **2016**, *21*, 547.

(24) Hu, Y.; Yang, D.; Huang, S. Amorphous photonic structures with brilliant and noniridescent colors via polymer-assisted colloidal assembly. *ACS Omega* **2019**, *4*, 18771−18779.

(25) Goerlitzer, E. S. A.; Klupp Taylor, R. N.; Vogel, N. Bioinspired photonic pigments from colloidal self-assembly. *Adv. Mater.* **2018**, *30*, 1706654.

(26) Chen, S.; Lu, W.; Shen, H.; Xu, S.; Chen, X.; Xu, T.; Wang, Y.; Chen, Y.; Gu, Y.; Wang, C.; Wu, X.; Beller, M.; Chen, W. The development of new pigments: Colorful g-C_3N_4-based catalysts for nicotine removal. *Appl. Catal., B* **2019**, *254*, 500−509.

(27) Kuang, M.; Wang, J.; Bao, B.; Li, F.; Wang, L.; Jiang, L.; Song, Y. Inkjet printing patterned photonic crystal domes for wide viewing-angle displays by controlling the sliding three phase contact line. *Adv. Opt. Mater.* **2014**, *2*, 34−38.

(28) Yang, J.; Zhang, X.; Zhang, X.; Wang, L.; Feng, W.; Li, Q. Beyond the visible: bioinspired infrared adaptive materials. *Adv. Mater.* **2021**, *33*, 202004754.

(29) Cao, Y.; Li, Q.; Li, C.; Li, J.; Yang, J. Surface heterojunction between (001) and (101) facets of ultrafine anatase TiO_2 nanocrystals for highly efficient photoreduction CO_2 to CH_4. *Appl. Catal., B* **2016**, *198*, 378−388.

(30) Song, H.; Li, C.; Lou, Z. Effective formation of oxygen vacancies in black TiO_2 nanostructures with efficient solar-driven water splitting. *ASC Sustain. Chem. Eng.* **2017**, *5*, 8982−8987.

(31) Wu, X.; Lan, D.; Zhang, F. R.; Ge, J. Fabrication of opaline ZnO photonic crystal film and its slow-photon effect on photo-reduction of carbon dioxide. *Langmuir* **2019**, *35*, 194−202.
(32) Klement, P.; Anders, D.; Guembel, L.; Bastianello, M.; Michel, F.; Schörmann, J.; Elm, M. T.; Heiliger, C.; Chatterjee, S. Surface diffusion control enables tailored-aspect-ratio nanostructures in area-Selective tomiclayer deposition. *ACS Appl. Mater. Interfaces* **2021**, *13*, 19398−19405.
(33) Kafizas, A.; Kellici, S.; Darr, J. A.; Ivan, P. P. Titanium dioxide and composite metal/metal oxide titania thin films on glass: a comparative study of photocatalytic activity. *J. Photoch. Photobio. A* **2009**, *204*, 183−190.
(34) Zhang, K.; Park, J. Surface localization of defects in black TiO_2: enhancing photoactivity or reactivity. *J. Phys. Chem. Lett.* **2017**, *8*, 199−207.
(35) Lu, X.; Wang, G.; Zhai, T. Hydrogenated TiO_2 nanotube arrays for supercapacitors. *Nano Lett.* **2012**, *12*, 1690−1696.
(36) Zhang, R.; Zeng, F.; Pang, F.; Ge, J. Substantial enhancement toward the photocatalytic activity of CdS quantum dots by photonic crystal-supporting films. *ACS Appl. Mater. Interfaces* **2018**, *10*, 42241−42248.
(37) Liu, J.; Li, M.; Wang, J.; Song, Y.; Jiang, L.; Murakami, T.; Fujishima, A. Hierarchically macro-/ mesoporous Ti−Si oxides photonic crystal with highly efficient photocatalytic capability. *Environ. Sci. Technol.* **2009**, *43*, 9425−9431.
(38) Kim, H.; Kang, B.; Cui, X.; Lee, S. K.; Lee, W.; Cho, D.; Woonbong, H.; Tim, B. F.; Woodfield, K. S. L.; Jang, J. Light-activated decellularized extracellular matrix-based bioinks for volumetric tissue analogs at the centimeter scale. *Adv. Funct. Mater.* **2021**, *31*, 2104991.
(39) Wang, C.; Lin, X.; Schäfer, C.; Hirsemann, S.; Ge, J. Spray synthesis of photonic crystal based automotive coatings with bright and angular-dependent structural colors. *Adv. Funct. Mater.* **2021**, *31*, 2008601.
(40) Li, Q.; Zhang, Y.; Shi, L.; Qiu, H.; Zhang, S.; Qi, N.; Hu, J.; Wei, Y.; Zhang, X.; Zha, K. Additive mixing and conformal coating of noniridescent structural colors with robust mechanical properties fabricated by atomization deposition. *ACS Nano* **2018**, *12*, 3095−3102.
(41) Ge, D.; Yang, L.; Wua, G.; Yang, S. Spray coating of superhydrophobic and angle-independent coloured films. *Chem. Commun.* **2014**, *50*, 2469−2472.
(42) Pang, F.; Jiang, Y.; Zhang, Y.; He, M.; Ge, J. Synergetic enhancement of photocatalytic activity with a photonic crystal film as a catalyst support. *J. Mater. Chem. A* **2015**, *3*, 21439−21443.
(43) Zhu, H.; Zhang, Y.; Zhu, J.; Li, Y.; Jiang, S.; Wu, N.; Wei, Y.; Zhou, J.; Song, Y. Crack-free hematite inverse opal photo-anodes for enhancing photo-electrochemical water splitting. *J. Mater. Chem. A* **2020**, *8*, 22929−22937.
(44) Low, J.; Zhang, L.; Zhu, Z.; Liu, Li.; Yu, J. TiO_2 photonic crystals with localized surface photothermal effect and enhanced photocatalytic CO_2 reduction activity. *ASC Sustain. Chem. Eng.* **2018**, *6*, 15653−15661.
(45) Ge, B.; Han, L.; Gao, B.; Zhang, T.; Li, X.; Zhu, X.; Pu, X.; Li, W. A mesoporous SiO_2/TiO_2 composite used for various emulsions separation. *Sep. Sci. Technol.* **2019**, *54*, 962−969.
(46) Liu, L.; Wang, X.; Cheng, B.; Zhang, C. Modification of spherical SiO_2 particles via electrolyte for high zeta potential and self-assembly of SiO_2 photonic crystal. *J. Brazil. Chem. Soc.* **2009**, *20*, 46−50.
(47) Xuan, X.; Tu, S.; Yu, H.; Du, X.; Zhao, Y.; He, J.; Dong, H.; Zhang, X.; Huang, H. Size-dependent selectivity and activity of CO_2 photoreduction over black nano-titanias grown on dendritic porous silica particles. *Appl. Catal., B* **2019**, *255*, 117768.

https://doi.org/10.1021/acsomega.2c00346
ACS Omega 2022, 7, 12089−12097